GEOPHYSICS, VOL. 78, NO. 1 (JANUARY-FEBRUARY 2013); P. G1–G13, 7 FIGS.
10.1190/GEO2012-0196.1

Polynomial equivalent layer

Vanderlei C. Oliveira Jr.[1], Valéria C. F. Barbosa[1], and Leonardo Uieda[1]

ABSTRACT

We have developed a new cost-effective method for processing large-potential-field data sets via the equivalent-layer technique. In this approach, the equivalent layer is divided into a regular grid of equivalent-source windows. Inside each window, the physical-property distribution is described by a bivariate polynomial. Hence, the physical-property distribution within the equivalent layer is assumed to be a piecewise polynomial function defined on a set of equivalent-source windows. We perform any linear transformation of a large set of data as follows. First, we estimate the polynomial coefficients of all equivalent-source windows by using a linear regularized inversion. Second, we transform the estimated polynomial coefficients of all windows into the physical-property distribution within the whole equivalent layer. Finally, we premultiply this distribution by the matrix of Green's functions associated with the desired transformation to obtain the transformed data. The regularized inversion deals with a linear system of equations with dimensions based on the total number of polynomial coefficients within all equivalent-source windows. This contrasts with the classical approach of directly estimating the physical-property distribution within the equivalent layer, which leads to a system based on the number of data. Because the number of data is much larger than the number of polynomial coefficients, the proposed polynomial representation of the physical-property distribution within an equivalent layer drastically reduces the number of parameters to be estimated. By comparing the total number of floating-point operations required to estimate an equivalent layer via our method with the classical approach, both formulated with Cholesky's decomposition, we can verify that the computation time required for building the linear system and for solving the linear inverse problem can be reduced by as many as three and four orders of magnitude, respectively. Applications to synthetic and real data show that our method performs the standard linear transformations of potential-field data accurately.

INTRODUCTION

In accordance with potential theory, a discrete set of observations of a potential field produced by a 3D physical-property distribution can be exactly reproduced by a 2D physical-property distribution. This 2D physical-property surface distribution is continuous and infinite. In practice, it is approximated by a finite set of equivalent sources arranged in a layer with finite horizontal dimensions and located below the observation surface. Usually the equivalent sources are represented by magnetic dipoles, doublets, point masses, or more complex sources such as prisms. In the literature, this layer that is made up of equivalent sources is referred to as the equivalent layer (Dampney, 1969).

By following the classical approach of the equivalent-layer principle, the physical property of each equivalent source is estimated by solving a linear inversion subject to fitting a discrete set of potential-field observations. Next, the estimated 2D physical-property distribution can be used to perform any standard linear transformation of the potential-field data such as interpolation (e.g., Cordell, 1992; Mendonça and Silva, 1994), upward (or downward) continuation (e.g., Emilia, 1973; Hansen and Miyazaki, 1984; Li and Oldenburg, 2010) and reduction to the pole of magnetic data (e.g., Silva 1986; Leão and Silva, 1989; Guspí and Novara, 2009). Specifically, the desired linear transformation of the potential-field data can be obtained by multiplying the matrix of Green's functions associated with the desired transformation by the estimated physical-property distribution (magnetization-intensity or density distributions).

The advent of airborne surveys made possible the acquisition of a huge volume of potential-field observations. In a typical airborne

Manuscript received by the Editor 29 May 2012; revised manuscript received 28 August 2012; published online 11 December 2012.
[1]Observatório Nacional, Rio de Janeiro, Brazil. E-mail: vandscoelho@gmail.com; valcris@on.br; leouieda@gmail.com.

survey, these observations are collected every few meters, generating data sets that may contain hundreds of thousands observations (Uieda and Barbosa, 2012). Although airborne surveys provide high-resolution potential-field data, the processing of these large potential-field data sets may lead to costly computational schemes, such as the application of the equivalent-layer technique. Hence, the computational demand for performing discrete linear transformations of large potential-field data sets also increases. However, for processing a huge quantity of data via the equivalent-layer technique, a huge number of equivalent sources is required. Usually, the equivalent-layer technique requires several equivalent sources M greater than the number of observations N. The larger the number of equivalent sources, the smaller will be the dependence of the result on the type of source used (dipoles, prisms, etc.) and on the distribution of these sources within the equivalent layer. Thus, the use of a large number of equivalent sources increases the chance of the estimated physical-property distribution yields an acceptable data fit. On the other hand, a large number of equivalent sources makes the construction of the linear system and the solution of the resulting inverse problem prohibitively inefficient. Hence, the challenge for potential-field data processing via the equivalent-layer technique is that of a large-scale inversion. As properly pointed out by Barnes and Lumley (2011), the key to a successful equivalent-source processing scheme rests with carefully designed software that can handle large optimization problems efficiently. To overcome this difficulty, a few methods have been developed to make feasible the use of the equivalent-layer technique for processing large data sets.

Leão and Silva (1989) developed a fast method for performing any linear transformation of a large set of potential-field data using the equivalent-layer principle. These authors posed the linear inverse problem of estimating the physical properties of M equivalent sources from potential-field data in the data space. This leads to a linear system of equations with dimensions based on the number of data N, instead of the number of sources M. To greatly reduce the total processing time and memory requirements, Leão and Silva's (1989) method used a small, moving data window that is shifted over the whole gridded data set. By using the observations inside a small data window, Leão and Silva (1989) estimated the physical-property distribution of a set of equivalent sources forming a small equivalent layer. These authors set up an equivalent layer extending beyond the moving-data window and at a depth between two and six times the grid spacing of the observations. Next, they compute the transformed field at the center of the moving-data window only. This procedure is repeated for each position of a moving-data window that spans the data until the whole area is processed. Leão and Silva's (1989) method leads to a fast grid operator which is applied to the data by a procedure similar to a discrete convolution.

Mendonça and Silva (1994) developed the equivalent-data concept which makes the equivalent-layer technique a feasible interpolation method. The equivalent-data concept consists in determining a subset of all potential-field observations (named equivalent data) such that the estimated physical-property distribution within an equivalent layer that fits the determined subset also fits the remaining potential-field observations automatically. The authors also pointed out that the computational efficiency of the method depends on the number of equivalent data. If the potential-field anomaly is nonsmooth, the number of equivalent data can be large and the method will be less efficient than the classical approach.

Li and Oldenburg (2010) develop a rapid method for processing large potential-field data sets by using the equivalent-layer principle. Li and Oldenburg's (2010) method uses the sparse wavelet representation of the matrix of Green's functions whose jth column contains the potential-field contribution of the jth equivalent source, with unit physical property, at the positions where the observations were made. To obtain a sparse representation of the matrix of Green's functions, Li and Oldenburg (2010) apply the 2D wavelet transform to each row and column of this matrix and set to zero the wavelet coefficients that are below a given threshold. Finally, these authors estimate the physical-property distribution within an equivalent layer by using the conjugate gradient least-squares strategy. By comparing with the classical equivalent-layer approach, the authors pointed out that, given the compression, their method reduces the computational time required for solving the linear system by as many as two orders of magnitude.

Barnes and Lumley (2011) reduce the noise level by a factor of 2.4 of the g_{zz} component of the gravity gradient tensor by using the equivalent layer technique. These authors grouped equivalent sources far from an observation point in blocks with average physical properties. This procedure aims at obtaining a linear system with a sparse matrix that reduces the memory storage and computational time. By using a weighted-least-squares conjugate-gradient strategy, Barnes and Lumley (2011) solved the resulting linear inverse problem.

We present a new fast method for processing large potential-field data sets by applying the equivalent-layer technique. Our method divides the equivalent layer into a regular grid of equivalent-source windows inside which the physical-property distribution is described by bivariate polynomial functions. This polynomial representation of the physical-property distribution within the equivalent layer considerably decreases the number of parameters to be estimated in the linear inverse problem. Our inverse problem is posed in the space of the total number of polynomial coefficients within all equivalent-source windows. This contrasts with the classical equivalent layer technique, derived through operations within the data or model spaces. By comparing the classical equivalent layer technique with our method and formulating the corresponding linear inverse problems using Cholesky's decomposition, we illustrate that our method substantially reduces the required memory storage and number of floating-point operations. Tests conducted with large synthetic gravity- and magnetic-data sets and with a real magnetic-data set over the Goiás Magmatic Arc (in central Brazil) show the good performance of our method in producing equivalent layers able to carry out the standard linear transformations of potential-field data without a prohibitively costly computational load.

METHODOLOGY

Classical approach

Let $\mathbf{d}$ be an N-dimensional vector of potential-field observations (gray dots in Figure 1a) and $\mathbf{p}$ be an M-dimensional vector of the equivalent sources' physical-property values. We assume that the M equivalent sources (black dots in Figure 1b) are distributed in a regular grid with a constant depth z_0 forming an equivalent layer. Usually, the equivalent sources can be either points of masses or dipoles, depending on whether the potential-field observations are gravity or magnetic data, respectively. Hence, $\mathbf{p}$ contains a set of M densities, in the case of gravity data, or magnetic intensities, in

the case of magnetic data. The potential field predicted by the equivalent layer at N observation points can be written in matrix notation as

$$\mathbf{g}(\mathbf{p}) = \mathbf{G}\mathbf{p}, \tag{1}$$

where $\mathbf{g}(\mathbf{p})$ is an N-dimensional vector whose ith element $g_i(\mathbf{p})$ is the potential-field data predicted at the ith observation point ($x = x_i$, $y = y_i$, and $z = z_i$, referred to a right-hand Cartesian coordinate system with the z-axis pointing downward (Figure 1a), and $\mathbf{G}$ is the $N \times M$ matrix of Green's functions, whose ijth element is the potential field at the ith observation point produced by the jth equivalent source located at $x = x'_j$, $y = y'_j$, and $z = z_0$ (Figure 1b), and with unitary physical property.

In applying the classical equivalent-layer technique, the parameters to be estimated are the physical properties (densities or magnetic intensities) of the M equivalent sources (e.g., point of masses or dipoles). The inverse problem of estimating this discrete physical-property distribution (the parameter vector $\mathbf{p}$ in equation 1) from observed data is an ill-posed problem because its solution is nonunique and unstable. In the classical equivalent-layer technique, a stable estimate of $\mathbf{p}$ can be obtained by using a parameter-space approach with the zeroth-order Tikhonov regularization (Tikhonov and Arsenin, 1977), i.e.,

$$\mathbf{p}^* = (\mathbf{G}^T\mathbf{G} + \mu\mathbf{I})^{-1}\mathbf{G}^T\mathbf{d}, \tag{2}$$

where the superscript T stands for a transpose, μ is a regularizing parameter and $\mathbf{I}$ is an identity matrix of order M. After estimating the vector $\mathbf{p}^*$, a desired linear transformation, such as interpolation, reduction to the pole and upward (or downward) continuation, is performed by

$$\mathbf{t} = \mathbf{T}\mathbf{p}^*, \tag{3}$$

where $\mathbf{t}$ is an N-dimensional vector containing the transformed field and $\mathbf{T}$ is an $N \times M$ matrix of Green's functions whose ijth element is the transformed field at the ith observation point (Figure 1a) produced by the jth equivalent source (Figure 1b) with unitary physical property. For example, if the desired transformation is an upward continuation of the gravity data, the ijth element of the matrix $\mathbf{T}$ is the gravity effect at the continuation height produced by the jth point of mass located at (x'_j, y'_j, z_0) and with unitary density.

A linear transformation through the equivalent-layer technique is performed in two steps: 1) estimating the physical-property distribution (equation 2), and 2) performing a matrix-vector multiplication to obtain the transformed field (equation 3). In terms of computational load, the first step is the biggest obstacle in using the equivalent-layer technique. This step requires the solution of a large linear system (equation 2) based on matrix $(\mathbf{G}^T\mathbf{G} + \mu\mathbf{I})$ with dimension $M \times M$. Hence, the computational problem in forming and inverting an $M \times M$ matrix is not feasible when the number of parameters is large. To avoid the dependence on the source pattern and on the spatial distribution of the sources within the equivalent layer, the equivalent-layer technique usually requires several equivalent sources M greater than the number of observations N, and thus, a large-scale inversion is expected.

Alternatively, a stable estimate of the parameter vector can be obtained by using a data-space approach with the zeroth-order Tikhonov regularization (Tikhonov and Arsenin, 1977), i.e.,

$$\mathbf{p}^* = \mathbf{G}^T(\mathbf{G}\mathbf{G}^T + \mu\mathbf{I})^{-1}\mathbf{d}, \tag{4}$$

where $\mathbf{I}$ is an identity matrix of order N. The data-space approach is computationally much more efficient than the parameter-space because it forms the $N \times N$ matrix $(\mathbf{G}\mathbf{G}^T + \mu\mathbf{I})$, instead of the $M \times M$ matrix in equation 2. To reduce even further the computational effort, $\mathbf{p}^*$ (equation 4) can be obtained in two steps. In the first one, we solve the linear system

$$(\mathbf{G}\mathbf{G}^T + \mu\mathbf{I})\mathbf{w} = \mathbf{d}, \tag{5}$$

where the vector $\mathbf{w}$ is a dummy variable. In the second step we evaluate

$$\mathbf{G}^T\mathbf{w} = \mathbf{p}^*. \tag{6}$$

Although formulating the equivalent-layer problem in the data space (equation 4) reduces significantly the size of the linear system to be solved compared with the parameter-space approach (equation 2), the computational effort is still excessive. In practice, this makes it unfeasible when dealing with large values of N (i.e., the number of data). To overcome this difficulty, we propose a new concept of equivalent layer that leads to a computationally efficient method to estimate $\mathbf{p}^*$.

Polynomial equivalent layer (PEL)

Let an equivalent layer be composed of M equivalent sources (black dots in Figure 1b) whose physical properties (densities or magnetic intensities) are the elements of an M-dimensional parameter vector $\mathbf{p}$. Here, the equivalent sources consist of magnetic dipoles or point of masses because they demand simple computer calculations. Let's divide this equivalent layer into Q equivalent-source windows (dashed rectangles in Figure 1b) with the same horizontal extensions and the same number M_s of equivalent sources, where $M_s \ll M$ and $M = M_s \cdot Q$. Hence, we partition the parameter vector as $\mathbf{p} = [\mathbf{p}^{1^T} \ldots \mathbf{p}^{Q^T}]^T$, where $\mathbf{p}^k$, $k = 1, \ldots, Q$, is

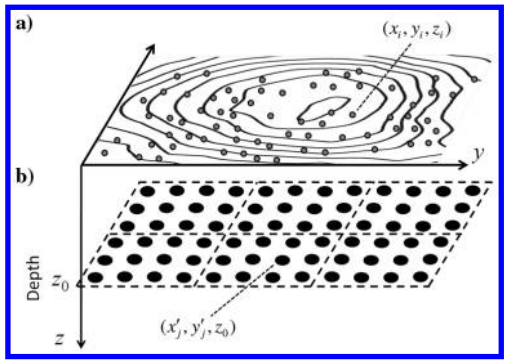

Figure 1. Schematic representation of the equivalent layer. (a) Observed potential-field anomaly (black contour lines) measured at a set of N observation points (gray dots) located at coordinates (x_i, y_i, z_i), $i = 1, \ldots, N$. (b) The equivalent layer is a thin slab in the subsurface which contains M fictitious equivalent sources (black dots) distributed in a grid at constant depth z_0. These sources are located at coordinates (x'_j, y'_j, z_0), $j = 1, \ldots, M$, and they can be point masses (in the case of gravity data) or dipoles (in the case of magnetic data). This equivalent layer is divided into Q equivalent-source windows (dashed rectangles).

an M_s-dimensional vector containing the physical properties of the equivalent sources within the kth equivalent-source window. Here, the physical-property distribution within the kth window is described by a bivariate polynomial q_k, $k = 1, ..., Q$, of degree α. The number P of constant coefficients of q_k is given by

$$P = \sum_{l=1}^{\alpha+1} l. \tag{7}$$

It follows that the physical-property values of the equivalent sources within the kth equivalent-source window $\mathbf{p}^k$ can be expressed in terms of the coefficients c_l^k, $l = 1, \ldots, P$, of the αth-order polynomial function q_k, i.e.,

$$\mathbf{p}^k = \sum_{l=1}^{P} \mathbf{b}_l^k c_l^k. \tag{8}$$

This linear relationship can be written in matrix notation as

$$\mathbf{p}^k = \mathbf{B}^k \mathbf{c}^k, \qquad k = 1, ..., Q, \tag{9}$$

where c^k is a $\mathbf{p}$-dimensional vector whose lth element c_l^k is the lth coefficient of the polynomial q_k, and $\mathbf{B}^k$ is an $M_s \times P$ matrix whose lth column is the M_s-dimensional vector $\mathbf{b}_l^k$. A generic element of matrix $\mathbf{B}^k$ is the first-order derivative of the αth-order polynomial function q_k with respect to one of the P coefficients $(c_1^k, ..., c_P^k)$. To illustrate this matrix, let's consider a kth equivalent-source window composed of $M_s = 12$ equivalent sources whose physical-property distribution can be described by a second-order polynomial ($\alpha = 2$ and $P = 6$, equation 7). In this case, the jth element of the 12×1 parameter vector $\mathbf{p}^k$ (equations 8 and 9) is

$$p_j^k = c_1^k + c_2^k x'_j + c_3^k y'_j + c_4^k x'^2_j + c_5^k x'_j y'_j + c_6^k y'^2_j, \quad j = 1, \ldots, 12 \tag{10}$$

and the 12×6 matrix $\mathbf{B}^k$ is

$$\mathbf{B}^k = \begin{bmatrix} 1 & x'_1 & y'_1 & x'^2_1 & x'_1 y'_1 & y'^2_1 \\ 1 & x'_2 & y'_2 & x'^2_2 & x'_2 y'_2 & y'^2_2 \\ \vdots & \vdots & \vdots & \vdots & \vdots & \vdots \\ 1 & x'_{M_s} & y'_{M_s} & x'^2_{M_s} & x'_{M_s} y'_{M_s} & y'^2_{M_s} \end{bmatrix}. \tag{11}$$

It is then clear that p_j^k, $j = 1, \ldots, 12$, is numerically equal to the second-order polynomial q_k evaluated at the horizontal coordinates (x'_j, y'_j) of the jth equivalent source within the kth equivalent-source window.

Here, the physical-property distribution within the equivalent layer is assumed to be a set of Q piecewise αth-order polynomial functions (i.e., q_k, $k = 1, ..., Q$) defined on a user-specified set of Q equivalent-source windows. Hence, the physical-property distribution of the entire equivalent layer, which includes all equivalent sources from all windows, can be described as

$$\mathbf{p} = \mathbf{B}\mathbf{c}, \tag{12}$$

where $\mathbf{B}$ is an $M \times H$ matrix ($H = P \cdot Q$) that can be partitioned as

$$\mathbf{B} = \begin{bmatrix} \mathbf{B}^1 & \mathbf{0} & \cdots & \mathbf{0} \\ \mathbf{0} & \mathbf{B}^2 & \cdots & \mathbf{0} \\ \vdots & \vdots & \ddots & \vdots \\ \mathbf{0} & \mathbf{0} & \cdots & \mathbf{B}^Q \end{bmatrix}, \tag{13}$$

where $\mathbf{0}$ is an $M_s \times P$ matrix of zeros. The H-dimensional vector $\mathbf{c}$ (equation 12) is partitioned as $\mathbf{c} = [\mathbf{c}^{1T} \ldots \mathbf{c}^{QT}]^T$. Hence, the vector $\mathbf{c}$ contains all coefficients describing all polynomial functions, q_k, $k = 1, ..., Q$, which are associated with the Q equivalent-source windows composing the entire equivalent layer.

By using equation 12, the linear system in equation 1, of N equations in M unknowns, can be rewritten as

$$\mathbf{g}(\mathbf{p}) = \mathbf{G}\mathbf{B}\mathbf{c}. \tag{14}$$

Equation 14 represents a system of N linear equations in H unknowns.

In our approach, named polynomial equivalent layer (PEL), we first solve the inverse problem of estimating the polynomial-coefficient vector $\mathbf{c}$ from the potential-field observations. Next, we calculate the physical-property distribution using equation 12. Finally, we compute the desired transformation of the data using equation 3. To obtain a stable estimate $\mathbf{c}$, we impose the zeroth- and first-order Tikhonov regularization (Tikhonov and Arsenin, 1977). Here, the linear inverse problem of estimating $\mathbf{c}$ is formulated as an optimization problem of minimizing

$$\frac{f_g}{H} \|c\|^2, \tag{15a}$$

and

$$\frac{f_g}{f_r} \|\mathbf{R}\mathbf{B}\mathbf{c}\|^2, \tag{15b}$$

subject to

$$\|\mathbf{g}(\mathbf{p}) - \mathbf{d}\|^2 = \delta, \tag{15c}$$

where $\|.\|$ is the Euclidean norm, δ is the expected mean square of the noise realizations in the data, and $\mathbf{R}$ is an $L \times M$ matrix representing a set of L first-order differences (Aster et al., 2004). The zeroth-order Tikhonov regularization (equation 15a) imposes that all coefficients estimates (vector $\mathbf{c}$) must be as close as possible to zero. The first-order Tikhonov regularization (equation 15b) imposes a smoothing constraint on estimated physical properties of the equivalent sources located at the boundary of adjacent windows. Finally, f_g and f_r are normalizing factors defined below.

By solving this constrained optimization problem (equation 15), we obtain the normal equation for the estimate $\mathbf{c}^*$, which is

$$\left[\mathbf{B}^T\mathbf{G}^T\mathbf{G}\mathbf{B} + \mu\left(\mu_0 \frac{f_g}{H}\mathbf{I} + \mu_1 \frac{f_g}{f_r}\mathbf{B}^T\mathbf{R}^T\mathbf{R}\mathbf{B}\right)\right]\mathbf{c}^* = \mathbf{B}^T\mathbf{G}^T\mathbf{d}, \tag{16}$$

where $\mathbf{I}$ is an identity matrix of order H and μ is the regularizing parameter that balances the relative importance between the data-misfit function (equation 15c) and the two constraints (equation 15a and 15b). The constants μ_0 and μ_1 (in equation 16) are real-positive numbers controlling the importance of the two constraints given by equation 15a and 15b, respectively. The normalizing factors f_g and f_r are the traces of the matrices $\mathbf{B}^T\mathbf{G}^T\mathbf{G}\mathbf{B}$ and $\mathbf{B}^T\mathbf{R}^T\mathbf{R}\mathbf{B}$, respectively.

Equation 16 represents a system of H linear equations in H unknowns, where H is the total number of polynomial coefficients forming all equivalent-source windows. This number of coefficients is much smaller than the number of equivalent sources M and the number of data N. Thus, the PEL requires much less computational effort than the classical equivalent-layer approach, even in the data-space formulation, which requires the solution of a system of N equations in N unknowns (equation 4). In our PEL algorithm, the full $N \times M$ matrix of Green's functions $\mathbf{G}$ and the full $M \times H$ matrix $\mathbf{B}$ (equation 13) are not stored; rather, only the small $H \times H$ matrix $\mathbf{B}^T\mathbf{G}^T\mathbf{G}\mathbf{B}$ (equation 16) is directly computed and stored. In our approach, the elements of the matrices $\mathbf{G}$ and $\mathbf{B}$ are computed on demand. We compute only the row of $\mathbf{G}$ and the column of $\mathbf{B}$ needed to calculate an element of the matrix $\mathbf{G}\mathbf{B}$. The same procedure is adopted to compute the $H \times H$ matrix $\mathbf{B}^T\mathbf{R}^T\mathbf{R}\mathbf{B}$ (equation 16). Once the vector $\mathbf{B}^T\mathbf{G}^T\mathbf{d}$ and the matrices $\mathbf{B}^T\mathbf{G}^T\mathbf{G}\mathbf{B}$ and $\mathbf{B}^T\mathbf{R}^T\mathbf{R}\mathbf{B}$ are computed, they are stored and then several reruns of the PEL program may be performed by setting different values for the inversion control constants (μ, μ_0 and μ_1, equation 16). The choice of these constants will be discussed later.

Computational efficiency of the PEL

The application of the equivalent-layer technique for processing potential-field data sets requires overcoming two main obstacles. The first one is the construction of the linear system. The second obstacle is the computational effort required to solve the resulting linear system. The PEL approach overcomes the first obstacle, mainly because of the sparseness of the matrix $\mathbf{B}$ (equation 13). The second obstacle is overcome by the PEL because it leads to a linear system of equations with dimensions based on the number of coefficients H within all equivalent-source windows, where H is much smaller than the number of parameters M and the data N. To illustrate the efficiency of the PEL when compared with the classical equivalent layer approach, we analyze below the total number of floating-point operations (flops) by solving the corresponding linear systems through Cholesky's decomposition.

Following Boyd and Vandenberghe (2004), we define a flop as an addition, subtraction, multiplication, or division of two floating-point numbers. In the classical equivalent-layer approach, the number of flops m_s required to solve the linear system (equation 5) by Cholesky's decomposition is

$$m_s = \frac{1}{3}N^3 + 2N^2. \tag{17a}$$

The construction of the linear system and the evaluation of the auxiliary operations (equation 6) requires m_c flops, where

$$m_c = MN^2 + 2NM, \tag{17b}$$

in which MN^2 and $2NM$ are the flops to evaluate $\mathbf{G}^T\mathbf{G}$ and equation 6, respectively. Thus, obtaining $\mathbf{p}^*$ by using the classical equivalent-layer approach posed in the data-space formulation (equations 5 and 6) requires $m_s + m_c$ flops.

Conversely, solving the resulting linear system in the PEL approach (equation 16) from Cholesky's decomposition requires h_s flops, where

$$h_s = \frac{1}{3}H^3 + 2H^2. \tag{18a}$$

By taking advantage of the sparseness in $\mathbf{B}$ (equation 13), the number of flops h_c required to construct the linear system and evaluate the auxiliary operations is given by

$$h_c = 2NM_sH + H^2N + 2NH + 2MP, \tag{18b}$$

where $2NM_sH$, H^2N, $2NH$, and $2MP$ are the number of flops required to evaluate the terms $\mathbf{G}\mathbf{B}$, $\mathbf{B}^T\mathbf{G}^T\mathbf{G}\mathbf{B}$, $\mathbf{B}^T\mathbf{G}^T\mathbf{d}$, and the physical-property distribution (the parameter vector $\mathbf{p}$ in equation 12), respectively. Notice that the use of zeroth-order Tikhonov regularization in the classical equivalent-layer approach (equation 4) and in the PEL approach (equation 16) demands, respectively, N and H addition operations; this is equivalent to adding N flops to m_c (equation 17b) and H flops to h_c (equation 18b). Because H is much smaller than N ($H \ll N$), the use of zeroth-order Tikhonov regularization in the PEL requires much less computational effort than in the classical equivalent-layer approach. On the other hand, the classical equivalent-layer approach (equations 2 and 4) does not use the first-order Tikhonov regularization. Thus, one might think that its use in the PEL (equation 16) would increase the number of flops h_c (equation 18b) because the demand of evaluating the term $\mathbf{B}^T\mathbf{R}^T\mathbf{R}\mathbf{B}$. This is not true because the sparseness of matrices $\mathbf{B}$ and $\mathbf{R}$ leads to a negligible increase of the h_c flops (equation 18b). Notice that the PEL requires the additional step of calculating the physical-property distribution (equation 12) after solving the linear system of equations to estimate the polynomial coefficients (equation 16). This must be done before computing the desired transformation of the data (equation 3). This additional step does not increase the computational cost significantly because computing the physical-property distribution (equation 12) only requires a sparse matrix-vector multiplication. To sum up, even using an additional regularizing function (equation 15b) and introducing an extra step in the processing workflow (equation 12), our equivalent-layer approach (PEL) requires a lower computational effort when compared with the classical equivalent-layer approach even using the N-dimensional-data-space formulation (equation 4).

We stress that the use of Cholesky's decomposition to solve the resulting linear system of equations for the PEL and the classical equivalent-layer approach is only taken as an example. Further optimization of the PEL approach is still possible by solving the linear system through a preconditioned conjugate gradient method. Regardless, the algorithm used to solve the linear system in the equivalent-layer problem, the H-dimensional system of equations to be solved by the PEL is always smaller than the N-dimensional system of equations required by the classical data-space approach. Ergo, solving $H \times H$ systems is much more efficient, in terms of time and memory requirements, than solving $N \times N$ systems.

PRACTICAL PROCEDURES

The practical procedures to use the PEL require the choice of two sets of variables. The first one is related to the geometry of the PEL and consists in choosing: (1) the depth to the equivalent layer (z_0), (2) the degree α of the polynomials describing the physical-property distribution within each equivalent-source window, (3) the size of the equivalent-source windows, (4) the number Q, and (5) the number M_s of equivalent sources forming each equivalent-source window. The second set of variables to be assigned is the inversion control constants (μ, μ_0 and μ_1, equation 16).

Choice of the geometry of the PEL

Compared with the fast Fourier transform filtering technique, methods that employ the equivalent-layer technique for processing potential-field data usually do not require gridded data. Likewise, our formulation (PEL) does not require gridded data. Conversely, a common restriction of methods that employ the equivalent-layer technique is that the vertical distance between the equivalent layer and the surface containing the potential-field observations must be between two and six times the grid spacing of the observations (Dampney, 1969; Leão and Silva, 1989). The applications of the PEL have not shown a strong dependence with respect to the vertical coordinate z_0 of the equivalent layer. In practice, the equivalent layer in our formulation can be placed at a constant-vertical position z_0 varying from about 150 to 300 m below the average height of the potential-field observations. Conversely, the dependence of the PEL on the size of the equivalent-source window and on the degree α of the polynomials is more critical. Moreover, the chosen size of the equivalent-source window will be strongly dependent on the choice of the degree α of the polynomials. Both choices must be grounded on the complexity of the potential-field anomalies. If the potential-field anomaly is characterized by long wavelength, we may use a large equivalent-source window and a high degree of the polynomial (e.g., $\alpha = 3$). Conversely, if the potential-field anomaly contains short-wavelength and high-amplitude components, we may use a small equivalent-source window and a low degree of the polynomial (e.g., $\alpha = 1$). This relation is illustrated later in the applications to synthetic and real data sets. A conservative practice when applying the PEL is to choose a small equivalent-source window and a low degree α of the polynomial. This conservative option is recommended when the potential-field anomaly contains long- and short-wavelength spectral contents. Additionally, we stress that this conservative choice works well even in the case of smooth anomalies with long-wavelength components only. Regardless of the chosen size of the equivalent-source window and degree α of the polynomials, the estimated physical-property distribution of the PEL must produce predicted data that fit the potential-field observations.

The division of the equivalent layer into Q equivalent-source windows consists of the following steps:

1) The interpreter must establish the smallest horizontal length L_s of a data square which contains a potential-field response with a short-wavelength. This square represents the area of an equivalent-source window.
2) The number of equivalent-source windows Q_x and Q_y in the x- and y-directions, respectively, are defined as

$$Q_x = \lceil (L_x/L_s) \rceil, \tag{19}$$

and

$$Q_y = \lceil (L_y/L_s) \rceil, \tag{20}$$

where L_x and L_y are the maximum horizontal lengths of the whole surveyed area in the x- and y-directions, respectively, and $\lceil\ \rceil$ is the ceiling function (Graham et al., 1988), which is defined as the least integer greater than or equal to its argument.

3) The number of equivalent-source windows Q is defined as

$$Q = Q_x \cdot Q_y. \tag{21}$$

4) Within each equivalent-source window, the number of equivalent sources in the x- and y-directions is the same and equal to

$$m = \left\lceil \sqrt{N/Q} \right\rceil, \tag{22}$$

where N is the number of potential-field observations.

5) Finally, the number of equivalent sources forming each equivalent-source window is defined as

$$M_s = m^2. \tag{23}$$

Choice of the inversion control constants

The choice of the values of inversion control constants (μ, μ_0, and μ_1, equation 16) is required to obtain a stable physical-property distribution via PEL. In practice, the value assigned to the regularizing parameter μ is one. The values assigned to μ_0 and μ_1 are selected in such a way that the estimated physical-property distribution is stable and fits acceptably the observed data. If the values of μ_0 and μ_1 are poorly assigned, the estimated physical-property distribution within the equivalent layer does not fit the data.

We adopted the following practical procedure to choose μ_0 and μ_1. Starting with small tentative values of μ_0 and μ_1, we estimate the physical-property distribution within the equivalent layer through the PEL approach (equations 16 and 12). If this estimate yields an unacceptable data fit, the value of μ_0 is maintained, the value of μ_1 is increased (by multiples of 10), and the PEL algorithm is rerun (equation 16) to estimate a new physical-property distribution (equation 12). In the following numerical applications, μ_1 is defined in the range of $10^{-7} \leq \mu_1 \leq 10^{-1}$ and μ_0 is kept fixed at a very small value such as 10^{-15}.

These constants can be easily tuned through trial and error because, as pointed out before, our equivalent-layer method (PEL) is computationally efficient by solving a small H-dimensional system of equations. Furthermore, after computing the vector $\mathbf{B}^T\mathbf{G}^T\mathbf{d}$ and the matrices $\mathbf{B}^T\mathbf{G}^T\mathbf{GB}$, and $\mathbf{B}^T\mathbf{R}^T\mathbf{RB}$ (equation 16), they are stored and then several reruns of the PEL algorithm may be performed by setting different values for the inversion control constants (μ_0 and μ_1, equation 16).

APPLICATION TO SYNTHETIC DATA

We illustrate the use of the PEL approach in processing synthetic gravity and magnetic data produced by simulated bodies. In applying the PEL approach to synthetic gravity data, we perform an upward continuation of the data set. In the application to synthetic

magnetic data, the PEL approach is used to obtain the reduced-to-the-pole field.

Synthetic-gravity data set

We simulate a set of $N = 10{,}000$ noise-corrupted gravity observations (black lines and grayscale map in Figure 2a), computed on a plane at $z = -150$ m. The observations are produced by multiple sources (not shown) and are simulated on unevenly spaced stations. We corrupted the theoretical anomaly with zero-mean Gaussian pseudorandom noise with a standard deviation of 0.1 mGal. We set up a PEL with $M = 10{,}000$ equivalent sources (point masses) distributed on a regular grid at constant depth $z_0 = 200$ m. We divide this equivalent layer into $Q = 100$ equivalent-source windows

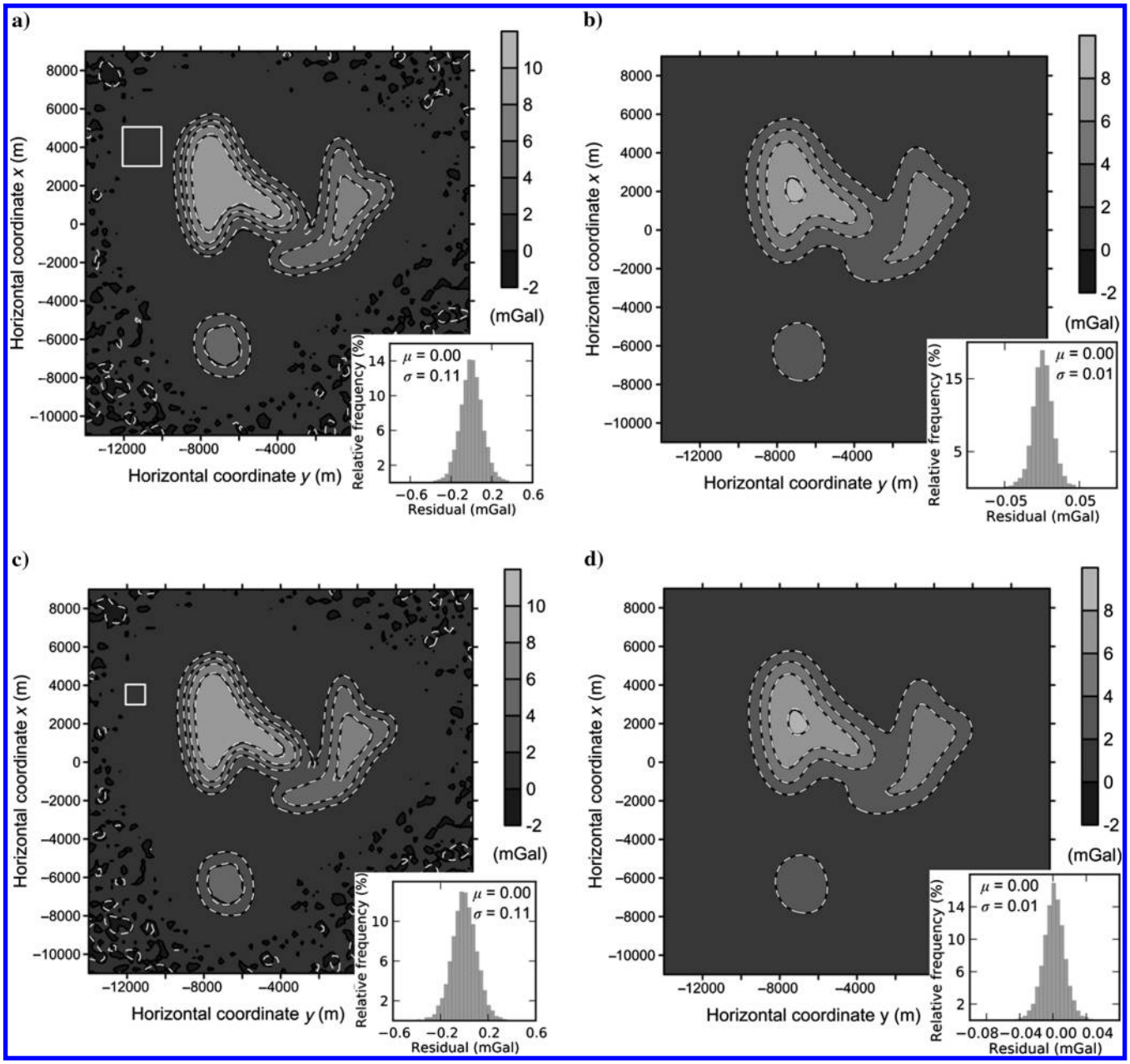

Figure 2. Tests with synthetic gravity data. (a) Simulated noise-corrupted (black lines and gray-scale map) and predicted (dashed white lines) gravity anomalies at $z = -150$ m; the latter is obtained by the estimated PEL using large-equivalent-source windows and third-order polynomials ($\alpha = 3$). (b) Simulated noise-free (black lines and grayscale map) and upward-continued (dashed white lines) anomalies at $z = -500$ m. The latter is obtained using the PEL estimated from the anomaly shown in (a) with large-equivalent-source windows and third-order polynomials ($\alpha = 3$). (c) Simulated noise-corrupted (black lines and grayscale map) and predicted (dashed white lines) gravity anomalies at $z = -150$ m. The latter is obtained through the PEL estimated using small-equivalent-source windows and first-order polynomials ($\alpha = 1$). (d) Simulated noise-free (black lines and grayscale map) and upward-continued (dashed white lines) anomalies at $z = -500$ m. The latter is obtained by using the PEL estimated from the anomaly shown in (c) with small-equivalent-source windows and first-order polynomials ($\alpha = 1$). The equivalent-source windows used in (a and b) and (c and d) are projected, respectively, onto (a and c) (outlined white rectangles). Histograms of the data misfits are shown as insets in (a-d) with their corresponding means μ and standard deviations σ.

arranged in a grid of 10×10 windows, each containing $M_s = 100$ equivalent sources. The area of an equivalent-source window is shown projected onto the data as the white open rectangle in Figure 2a. We used third-order polynomials ($\alpha = 3$) with $P = 10$ coefficients each (equation 7), totaling $H = 1000$ unknown coefficients which describe all Q polynomials that compose the equivalent layer. By setting $\mu_0 = 10^{-15}$ and $\mu_1 = 10^{-7}$, the estimated H coefficients ($\mathbf{c}^*$ in equation 16 are used to compute an estimated density distribution ($\mathbf{p}$, in equation 12) in the equivalent layer. This layer produces a predicted gravity data set at $z = -150$ m (in dashed white lines) which fits the simulated gravity data (in black lines and grayscale map) as shown in Figure 2a. Figure 2b shows that the gravity data continued to a constant-vertical coordinate $z = -500$ m using the estimated PEL (dashed white lines) agree very well with the true data computed at the same continuation height (black lines and grayscale map). Histograms of the data misfits (insets of Figure 2a and 2b) corroborate the acceptance of the data fitting. In both histograms, most of the data misfits are smaller than the one standard deviation of the observational uncertainty being consistent with a normal distribution.

In this test, the efficiency of the PEL approach comes from solving a 1000×1000 system versus a $10{,}000 \times 10{,}000$ system required by the classical equivalent-data approach in the data space. By using Cholesky's decomposition as the algorithm for solving the linear systems, the number of flops required by the classical approach to solve the linear system (equation 17a) is approximately 994 times greater than that required by the PEL (equation 18a). Additionally, the construction of the linear systems (equations 17b and 18b) requires approximately 83 times more flops for the classical approach than that for the PEL.

In the previous section, we presented the practical procedures of choosing (1) the degree α of the polynomials describing the physical-property distribution within each equivalent-source window and (2) the size of the equivalent-source window. According to the criterion described in the previous section, if the potential-field anomaly is dominated by long-wavelength spectral content (a smooth anomaly) there are two options: first, using a large equivalent-source window and a high degree α of the polynomial, as in the application to synthetic-gravity data set presented above (Figure 2a and 2b); second, using a small equivalent-source window and a low degree of the polynomial, following a conservative practice. To illustrate this conservative practice, we reproduced the previous application to synthetic-gravity data, only this time dividing the equivalent layer into $Q = 400$ equivalent-source windows arranged in a grid of 20×20 windows, each containing $M_s = 25$ equivalent sources. The white open rectangle in Figure 2c represents the projection of the area of the equivalent-source window onto the data. Additionally, we used first-order polynomials ($\alpha = 1$) with $P = 3$ coefficients, totaling $H = 1200$ unknown coefficients which describe all Q polynomials within the equivalent layer. This estimated equivalent layer produces a predicted gravity data set (dashed white lines) which fits the simulated gravity data (black lines and grayscale map). The gravity data continued to a constant-vertical coordinate $z = -500$ m using the estimated PEL (dashed white lines in Figure 2d) fit the true data computed at the same continuation height (black lines and grayscale map in Figure 2d) equally well when compared with the previous result (Figure 2b). This shows the excellent performance of our method in upward-continuing the gravity data to an elevation of -500 m by using a conservative choice of the size of the equivalent-source window and the degree α of the polynomials. Histograms of the data misfits (insets of Figure 2c and 2d) resemble bell-shaped distributions confirming that the simulated measurement errors are normally distributed. In this test, we set $\mu_0 = 10^{-15}$ and $\mu_1 = 10^{-7}$.

Regarding the computational performance, the PEL leads to computational efficiency by dealing with a 1200×1200 system versus a $10{,}000 \times 10{,}000$ one. By solving the resulting linear systems through Cholesky's decomposition, the number of flops required by the classical approach to solve and build the linear system is 576 times and 67 times greater than that required by the PEL, respectively. Thus, we verify that the PEL still provides a significant increase in performance, even if using a conservative choice of the size of the equivalent-source window and of the degree α of the polynomials.

Efficiency versus data-misfit measure

As pointed out in the methodology section, PEL greatly reduces the linear system of equations to be solved by representing the physical-property distribution within the equivalent layer as a set of piecewise-polynomial functions. By taking a fixed size of equivalent-source window, the smaller the degree α of the polynomial the smaller the number of the coefficients to be estimated ($\mathbf{c}^*$ in equation 16), hence the smaller the H-dimensional system of equations to be solved by PEL and the faster the inversion will be. Then, it would be always desirable to use low-degree polynomials. This is true (or not), depending on whether the estimated physical-property distribution yields an acceptable (or unacceptable) data fit.

As discussed in the practical procedures section, PEL depends on the choice of the size of the equivalent-source window and on the choice of the degree α of the polynomials. For a chosen size of the equivalent-source window, we can access the optimum degree α of the polynomials. The optimum value for α is the smallest one still producing an acceptable data fit. This criterion ensures a maximum computational efficiency and a satisfactory data fitting. Thus, there is a trade-off between the computational efficiency and the data-misfit measure obtained by assigning different values of α, for a given fixed size of the equivalent-source window in applying PEL approach.

Here, we analyze the trade-off between the data-misfit measure and the computational efficiency of our equivalent-layer approach (PEL) by assigning different degrees α of the polynomials, for a given fixed size of the equivalent-source window. Figure 3 shows two curves plotted against α: (1) the data-misfit measure (dashed line) and (2) the computational efficiency (solid line) of our equivalent-layer approach (PEL). These curves were computed by assuming the same size of the equivalent-source window shown in Figure 2a (white open rectangle). The computational efficiency of our equivalent-layer approach (PEL) is computed by the ratio N/H which represents a compression ratio of the linear system. We pointed out in the methodology section that small values of H lead to a great reduction of the size of the linear system to be solved through PEL (equation 16). For increasingly higher values of α, the values of H increase and the computational efficiency of PEL becomes increasingly lower. Hence, the computational efficiency of PEL (N/H) decreases with increasing α.

The optimum value for α, for a given fixed size of the equivalent-source window, is the smallest one still producing an acceptable data fit. This choice ensures the best computational efficiency of

PEL in addition to fitting the geophysical observations. In Figure 3, the optimum value of α is three, which is the value used in Figure 2a and 2b. The data-misfit measure is computed as the square of the Euclidean norm of the residual between the observed and fitted data divided by the number of observations. Depending on the size of the equivalent-source window used, values from α different of the optimum value produce a poor data fit increasing the data-misfit measure. Values of α smaller than optimum value (e.g., $\alpha < 3$ in Figure 3) produce a poor data fit, increasing the data-misfit measure. This occurs because the size of the equivalent-source window is large and the low-degree polynomial used is not able to estimate a physical-property distribution (equations 16 and 12) that acceptably fits the data. Hence, the estimate a physical-property distribution within the equivalent layer is roughly represented by piecewise αth-order polynomial functions defined on a set of equivalent-source windows. Conversely, values of α larger than an optimum value (e.g., $\alpha > 3$ in Figure 3) produce a poor data fit, increasing the data-misfit measure. This behavior occurs in PEL because the inverse problem becomes ill-posed and, consequently, the tuning of the inversion control constants (μ_0 and μ_1, equation 16) becomes difficult. Figure 3 illustrates the best trade-off between data-misfit measure (dashed line) and computational efficiency (solid line) of PEL in which $\alpha = 3$ is the optimal balance of these two terms.

Synthetic-magnetic data set

In this test, we simulate a complex magnetic response containing short-, mid-, and long-wavelength spectral contents. Because of this wide range of spectral contents, we must use a polynomial with a low degree ($\alpha = 1$) and a small equivalent-source window whose size is able to contain the shortest wavelength of the simulated anomaly. As pointed out, the size of the equivalent-source window can be easily chosen. Here, we illustrate how we can check if this size was suitably chosen. To this end, we apply the PEL by setting large- and small-equivalent-source windows which illustrate, respectively, unsuitable and suitable windows.

Figure 4 shows the noise-corrupted total-field anomaly (black contour lines) produced by a set of synthetic bodies (not shown). We corrupted the theoretical anomaly with zero-mean Gaussian pseudorandom noise with a standard deviation of 5 nT. We simulated an airborne magnetic survey covering an area with an extent of 10,000 km in the x- and y-directions (north–south and east–west, respectively). The flight height is 150 m above the ground surface. The simulated flight pattern contains 50 flight-lines along north–south direction with line spacing of 200 m and two tie-lines along the east–west direction with line spacing of 4000 m. Based on an average 270 km/h aircraft speed, the sampling frequency is 10 Hz and the number of data points per flight-line is 1333. The number of observations along the north–south and east–west are, respectively, 66,650 and 2666, totaling 69,316 observations. The simulated geomagnetic field has 45° declination and −3° inclination. The simulated bodies (not shown) are magnetized uniformly, with a magnetization declination of −10° and inclination of 2°. Notice that the spectral content of the magnetic response ranges from short to long wavelengths. At the northwestern (A) and easternmost (B) portions of the total-field anomaly map (Figure 4 in black contour lines), the magnetic responses are characterized predominantly by short- and long-wavelength spectral contents, respectively. Whereas, the magnetic response at the southernmost portion (C) contains mid-wavelength anomalies.

Large-equivalent-source window

We set up a PEL with $M = 74{,}529$ equivalent sources (magnetic dipoles) distributed on a regular grid at constant depth $z_0 = 200$ m. These magnetic dipoles have the same magnetization direction of the simulated body. This equivalent layer is divided into $Q = 169$ equivalent-source windows arranged in a grid of 13×13 windows, each one containing $M_s = 441$ equivalent sources arranged in a grid of 21×21 dipoles. The black open rectamgle in Figure 4a shows the area of an equivalent-source window projected onto the data set. We used first-order polynomials ($\alpha = 1$) with $P = 3$ coefficients (equation 7), totaling $H = 507$ unknown coefficients which describe all Q polynomials composing the equivalent layer. In this test, we set $\mu_0 = 10^{-15}$ and $\mu_1 = 10^{-1}$. After estimating the H coefficients (equation 16), we compute the magnetization-intensity distribution in the equivalent-source layer (equation 12) as show in Figure 5a. We also compute the predicted total-field anomaly (not shown) yielded by the magnetization-intensity distribution (Figure 5a) obtained through the PEL using a large equivalent-source window. Figure 4a shows the differences (colorscale map) between the simulated noise-corrupted (black contour lines) and predicted (not shown) total-field anomalies at $z = -150$ m. For most of the area, these differences are around zero nT. Larger differences (smaller than −60 nT or greater than 60 nT) coincide exclusively with the region where the magnetic responses are characterized mainly by short-wavelength spectral contents (region A in Figure 4a). In this test, this poor data fit produced by the PEL occurs because of the low-degree polynomial combined with the large-equivalent-source window. This combination leads to a rough estimate of physical-property distribution (Figure 5a) within the equivalent layer. Because of this unacceptable anomaly fit, the choice of the size of the equivalent-source window (black open rectangle in Figure 4a) is considered unsuitable and the transformation of the data will not be done. In this case, the size of the equivalent-source window must be reduced until an acceptable data fit is obtained.

Small-equivalent-source window

We set up a PEL with $M = 75{,}625$ equivalent sources (magnetic dipoles) distributed on a regular grid at constant depth $z_0 = 200$ m. These magnetic dipoles have the same magnetization direction of

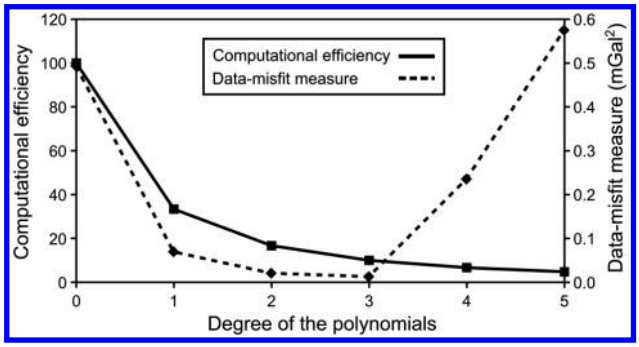

Figure 3. The trade-off between the data-misfit measure and the computational efficiency of PEL by assigning different degrees α of the polynomials. The data-misfit measure (dashed line) and the computational efficiency (solid line) of PEL were computed by assuming the same size as the equivalent-source window shown in Figure 2a (white open rectangle).

the simulated body. This equivalent layer is divided into $Q = 625$ equivalent-source windows arranged in a grid of 25×25 windows, each one containing $M_s = 121$ equivalent sources arranged in a grid of 11×11 dipoles. The black open rectangle in Figure 4b shows the area of an equivalent-source window projected onto the data set. We set $\mu_0 = 10^{-15}$ and $\mu_1 = 10^{-1}$. We used first-order polynomials ($\alpha = 1$) with $P = 3$ coefficients (equation 7), totaling $H = 1875$ unknown coefficients that describe all Q polynomials composing the equivalent layer. After estimating the H coefficients, we compute the magnetization-intensity distribution in the equivalent-source layer (Figure 5b). By setting a small-equivalent-source window in applying PEL, the differences (colorscale map in Figure 4b) between the simulated noise-corrupted (black contour lines in Figure 4b) and predicted (not shown) total-field anomalies at $z = -150$ m are much smaller than those obtained by setting a large-equivalent-source window (colorscale map in Figure 4a). This excellent data fit produced by the PEL (colorscale map in Figure 4b) is due to the combination of the low-degree polynomial and the small-equivalent-source window. This combination allows estimating a smoother magnetization-intensity distribution (Figure 5b) within the equivalent layer as compared with the distribution estimated by setting a large-equivalent-source window (Figure 5a). Histograms of the data misfits shown as insets of Figure 4a and 4b quantifies the poor and acceptable data fits produced by the PEL using large- and small-equivalent-source windows, respectively.

Because the data fitting is acceptable, the estimated magnetization-intensity distribution must be accepted and then the desired transformation of the data can be done. Hence, we used the equivalent layer estimated using the PEL to compute the reduced-to-the-pole anomaly (dashed white lines in Figure 6), which shows a close agreement with the true reduced-to-the-pole anomaly (black lines

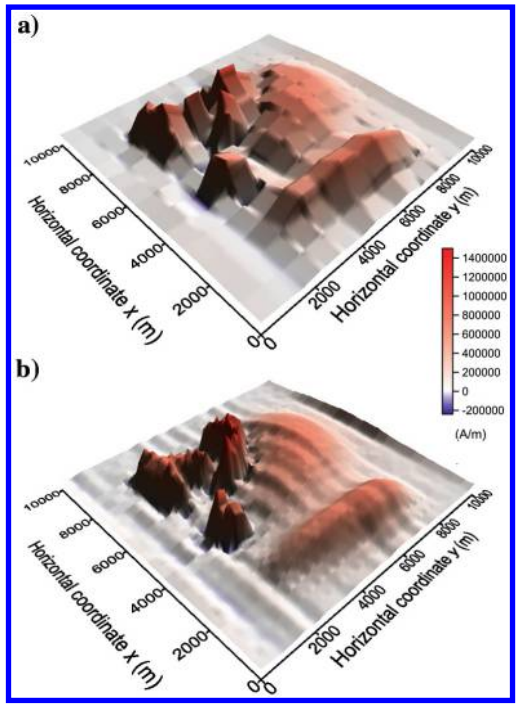

Figure 5. Tests with synthetic magnetic data. Computed magnetization-intensity distributions obtained by PEL with first-order polynomials ($\alpha = 1$) and large (a) and small (b) equivalent-source windows. The equivalent-source windows used in (a) and (b) are depicted in Figure 4a and 4b, respectively.

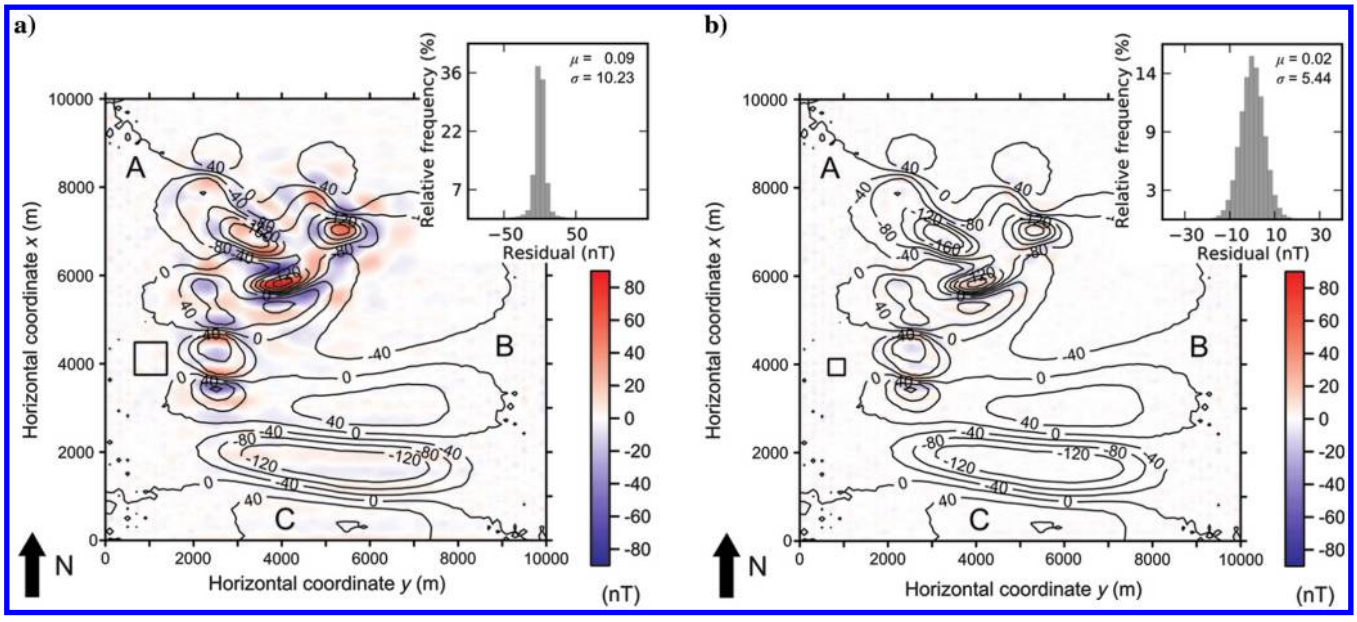

Figure 4. Tests with synthetic magnetic data. (a and b) Simulated noise-corrupted (black lines) total-field anomaly at $z = -150$ m characterized by short- (region A), mid- (region C), and long- (region B) wavelength spectral contents. The predicted total-field anomalies at $z = -150$ m (not shown) are obtained by the estimated PEL (shown in Figure 5) using first-order polynomials ($\alpha = 1$) and large (a) and small (b) equivalent-source windows. Color-scale maps in (a and b) show the differences between the simulated and predicted total-field anomalies. The equivalent-source windows used in (a and b) are projected onto the data set (outlined black rectangles). Histograms of the data misfits are shown as insets in (a and b) with their corresponding means μ and standard deviations σ.

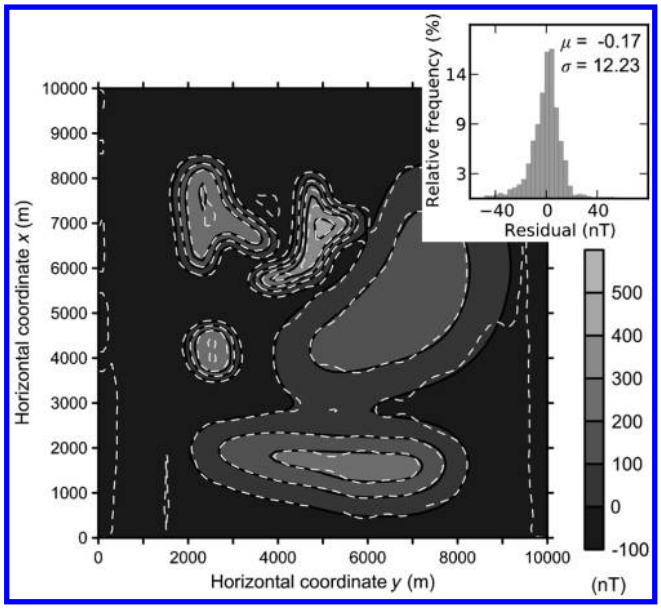

Figure 6. Test with synthetic magnetic data. Noise-free total-field anomaly at the pole (black lines and grayscale map) produced by the same set of simulated bodies described in Figure 4 and reduced-to-the-pole anomaly (dashed white lines) predicted by the estimated PEL shown in Figure 5b by using equivalent-source windows shown in Figure 4b. The inset shows the histogram of the residuals between the true noise-free anomaly at the pole and the reduced-to-the-pole anomaly predicted by the PEL with its mean μ and standard deviation σ.

and gray-scaled map in Figure 6). The histogram of the data misfits (inset of Figure 6) quantifies this agreement. The PEL approach solves a reduced system of equations (1875×1875 system) whereas the classical equivalent-data approach should solve a large system ($69{,}316 \times 69{,}316$ system). By using Cholesky's decomposition as the algorithm for solving the linear systems, the number of flops required by the classical approach to solve the linear system (equation 17a) is approximately 50,354 times greater than that required by the PEL (equation 18a). The construction of the linear system (equations 17b and 18b) requires approximately 1319 times more flops for the classical approach than for the PEL.

APPLICATION TO REAL DATA

We apply our method (PEL) to process an aeromagnetic data set over the Goiás Magmatic Arc, in central Brazil. This region is mainly made up of metaplutonic rocks exposed between volcano-sedimentary sequences (Pimentel et al., 2000). The aeromagnetic data set covers the southern portion of the Goiás Magmatic Arc at the Arenópolis Arc (Figure 7a) and was acquired at an average height of $z = -746$ m. The geomagnetic field has $-19°$ declination and $-21.5°$ inclination and we assume that the source has a total magnetization vector with $-19°$ declination and $-40°$ inclination based on Dutra and Marangoni (2009). The data set used contains $N = 78{,}146$ observations. We set up a PEL with $M = 81{,}000$ equivalent sources (dipoles) with $-19°$ declination and $-40°$ inclination and distributed on a regular grid at constant height $z_0 = -400$ m. We divide this equivalent layer into $Q = 810$ equivalent-source windows arranged in a grid of 27×30 windows, each one with $M_s = 100$ dipoles. The area of an equivalent-source window is projected onto the data set being outlined by the white open rectangle in Figure 7a. We used first-order polynomials ($\alpha = 1$)

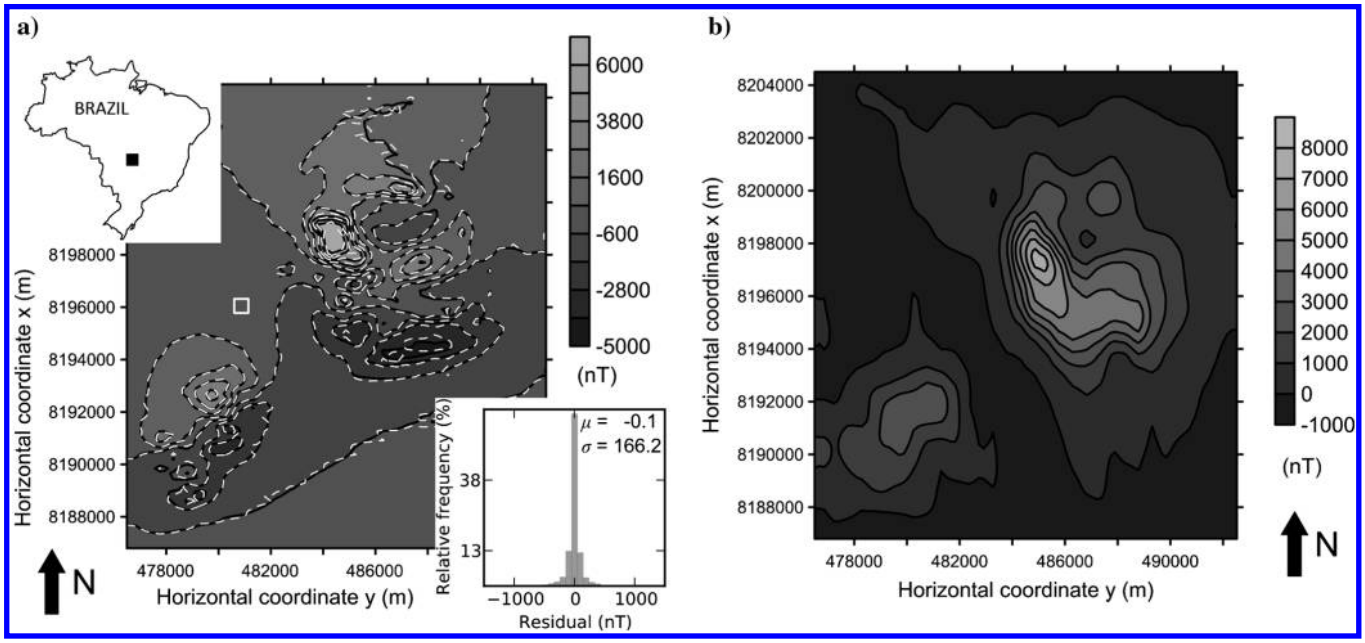

Figure 7. Real test from Arenópolis Arc (Brazil). (a) Observed (black lines and grayscale map) and predicted (dashed white lines) total-field anomalies. The latter is obtained by the estimated PEL (not shown). The inset on the right shows the histogram of the data misfit with its mean μ and standard deviation σ. The equivalent-source windows used are projected onto the data set (outlined white rectangle). The study area (black square) is shown as an inset in the map of Brazil. (b) Transformed data produced by applying the upward continuation and the reduction to the pole via the estimated PEL to the anomaly shown in (a).

with $P = 3$ coefficients (equation 7). Therefore, the number of unknown coefficients describing the magnetization intensities of the dipoles is $H = 2430$. We set $\mu_0 = 10^{-15}$ and $\mu_1 = 10^{-7}$. Figure 7a shows that the predicted total-field anomaly (dashed white lines) obtained by the PEL fits the observed total-field anomaly (black lines and grayscale map). The histogram of the data misfit (inset of Figure 7a) resembles a bell-shaped distribution confirming that the measurement errors are normally distributed with a small standard deviation. Next, we use the estimated PEL to compute the reduction to the pole of the aeromagnetic data at a z-coordinate -1300 m. Figure 7b shows the observed total-field anomaly upward-continued and reduced to the pole. We verify that our approach performed a meaningful reduction to the pole because the resulting reduced-to-the-pole anomaly (black lines and grayscale map in Figure 7b) is predominantly positive.

In this test, the PEL is computationally efficient because it deals with a 2430×2430 system instead of a $78{,}146 \times 78{,}146$ one. By solving the resulting linear systems through Cholesky's decomposition, the number of flops required by the classical approach (equation 17a) is approximately 33,179 times greater than that required by the PEL (equation 18a). The construction of the linear system (equations 17b and 18b) requires approximately 992 times more flops for the classical approach than for the PEL.

CONCLUSIONS

We have presented a new fast method for processing large sets of potential-field data via the equivalent-layer technique. The novelty of our method consists in dividing the equivalent layer into a regular grid of equivalent-source windows, whose physical-property distributions are described by bivariate polynomials. Thus, we assumed that the physical-property distribution within the equivalent layer can be described by a piecewise-polynomial function. After setting the size of equivalent-source window and the degree of the polynomial, our method estimates the polynomial coefficients for each window by using a regularized potential-field inversion. Next, the physical-property distribution within an equivalent layer is obtained by means of a transformation which maps the estimated polynomial coefficients into the physical-property distribution. Finally, the transformation of the data is performed by premultiplying the determined physical-property distribution by the matrix of Green's functions associated with the desired transformation.

The proposed polynomial representation of the physical-property distribution within the equivalent layer leads to a drastic reduction of the linear system of equations that needs to be solved for estimating this physical-property distribution compared with the classical equivalent-layer technique. This occurs because, in the classical equivalent-layer technique, the inverse problem of estimating the physical-property distribution within the equivalent layer is posed in the data space. In this case, the inverse problem leads to a linear system of equations with dimensions based on the number of data, N. In contrast, the inverse problem of our method leads to a linear system of equations with dimensions based on the total number of polynomial coefficients within all equivalent-source windows, which is significantly smaller than N. Conversely, the PEL requires an additional step of converting the estimated coefficients into the physical-property distribution within an equivalent layer. However, this does not imply a meaningful increase of the computational cost. This occurs because the transformation for mapping the estimated polynomial coefficients into the physical-property distribution is a linear function which involves only a sparse matrix-vector multiplication.

Applications to synthetic and real data sets show that our method produces effective equivalent-source layers for performing any linear transformation of potential-field data without a huge computational load and a long processing time as compared with the classical approach. One might think that the choices of the size of the equivalent-source window and of the degree of the polynomials would be a difficult task. However, a simple criterion that may be used is that the shorter the wavelength components of the potential-field anomaly, the smaller the size of the equivalent-source window and the lower the degree of the polynomial should be. A conservative choice is to use a small equivalent-source window and a low degree polynomial. A simple and effective way to check if the choices of the size of the equivalent-source window and the degree of the polynomial were correctly done consists in verifying if the estimated physical-property distribution via the PEL yields an acceptable data fit. If the data fitting is poor, the estimated physical-property distribution via PEL must be rejected and a smaller size of the equivalent-source window and (or) another degree of the polynomial must be tried. This procedure is repeated until an acceptable data fit is obtained. Thus, a poor fit of the observed data may be used as a criterion to evaluate the optimum size of the equivalent-source window and the optimum degree of the polynomial.

Further improvements in the methodology of the PEL could be attained by combining the division of the equivalent layer into a nonregular set of equivalent-source windows with the use of different degrees of the polynomials. This improvement could be implemented accordingly to the spectral content of the potential-field anomaly. The number of equivalent-source windows should be greater and the degree of the polynomial function should be lower where the data are characterized by short-wavelength components. Another improvement in the PEL methodology could be accomplished by using a moving-data-window scheme that is shifted over the whole data set. When inverting the observations inside a small data window by using a small equivalent-source located below the data window, only the transformed field near the center of the data window can be computed. Yet another improvement in the PEL methodology could be formulated by setting up an equivalent layer with a continuous distribution of the physical property which varies horizontally according to a piecewise-polynomial function. Hence, the potential-field forward problem could be numerically computed through Gaussian quadrature, for example.

Further computational efficiency of the PEL algorithm might be achieved by using different methods for solving the linear system. Here, we have used Cholesky's decomposition, however other algorithms could be employed such as the preconditioned conjugate gradient method.

Additionally, in the case of full-tensor gradiometry, our method could be used for processing all components together in a joint scheme, because all observations derive from common sources. The application of our polynomial equivalent layer is extremely fast, making feasible the processing of the large data sets often encountered in airborne surveys through the equivalent-layer technique. However, our method fails to provide a significant performance increase when processing a small number of sparsely spaced potential-field observations, as is routinely encountered in localized ground based surveys. The practical implementation of

the proposed polynomial equivalent layer is straightforward and does not require supercomputers or data-compression algorithms.

ACKNOWLEDGMENTS

We thank Gary Barnes, Fernando Guspí, Changli Yao, and associate editor Xiong Li for helpful and constructive remarks. The authors were supported in this research by a fellowship (V.C.F. Barbosa) and a scholarship (V.C. Oliveira Jr.) from Conselho Nacional de Desenvolvimento Científico e Tecnológico (CNPq), Brazil. L. Uieda was supported by a scholarship from Coordenação de Aperfeiçoamento de Pessoal de Nível Superior (CAPES), Brazil. Additional support for the authors was provided by the Brazilian research agencies CNPq (grant no. 471693/2011-1) and FAPERJ (grant no. E-26/103.175/2011). The authors also thank the government of the state of Goiás, Brazil, for permission to use the real aeromagnetic data set.

REFERENCES

Aster, R. C., B. Borchers, and C. H. Thurber, 2004, Parameter estimation and inverse problems: Elsevier Academic Press.

Barnes, G., and J. Lumley, 2011, Processing gravity gradient data: Geophysics, **76**, no. 2, I33–I47, doi: 10.1190/1.3548548.

Boyd, S., and L. Vandenberghe, 2004, Convex optimization: Cambridge University Press.

Cordell, L., 1992, A scattered equivalent-source method for interpretation and gridding of potential-field data in three dimensions: Geophysics, **57**, 629–636, doi: 10.1190/1.1443275.

Dampney, C. N. G., 1969, The equivalent source technique: Geophysics, **34**, 39–53, doi: 10.1190/1.1439996.

Dutra, A. C., and Y. R. Marangoni, 2009, Gravity and magnetic 3D inversion of Morro do Engenho complex, central Brazil: Journal of South American Earth Sciences, **28**, 193–203, doi: 10.1016/j.jsames.2009.02.006.

Emilia, D. A., 1973, Equivalent sources used as an analytic base for processing total magnetic field profiles: Geophysics, **38**, 339–348, doi: 10.1190/1.1440344.

Graham, R. L., D. E. Knuth, and O. Patashnik, 1988, Concrete mathematics: Addison-Wesley.

Guspí, F., and I. Novara, 2009, Reduction to the pole and transformations of scattered magnetic data using Newtonian equivalent sources: Geophysics, **74**, no. 5, L51–L59, doi: 10.1190/1.3170690.

Hansen, R. O., and Y. Miyazaki, 1984, Continuation of potential fields between arbitrary surfaces: Geophysics, **49**, 787–795, doi: 10.1190/1.1441707.

Leão, J. W. D., and J. B. C. Silva, 1989, Discrete linear transformations of potential field data: Geophysics, **54**, 497–507, doi: 10.1190/1.1442676.

Li, Y., and D. W. Oldenburg, 2010, Rapid construction of equivalent sources using wavelets: Geophysics, **75**, no. 3, L51–L59, doi: 10.1190/1.3378764.

Mendonça, C. A., and J. B. C. Silva, 1994, The equivalent data concept applied to the interpolation of potential field data: Geophysics, **59**, 722–732, doi: 10.1190/1.1443630.

Pimentel, M. M., R. A. Fuck, H. Jost, C. F. Filho Ferreira, and S. M. Araújo, 2000, The basement of the Brasília Fold Belt and the Goiás Magmatic Arc, *in* U. G. Cordani, E. J. Milani, A. Thomaz Filho, and D. A. Campos, eds., Tectonic evolution of South America: 31st International Geological Congress, 195–230.

Silva, J. B. C., 1986, Reduction to the pole as an inverse problem and its application to low-latitude anomalies: Geophysics, **51**, 369–382, doi: 10.1190/1.1442096.

Tikhonov, A. N., and V. Y. Arsenin, 1977, Solution of ill-posed problems: Winston & Sons.

Uieda, L., and V. C. F. Barbosa, 2012, Robust 3D gravity gradient inversion by planting anomalous densities: Geophysics, **77**, no. 4, G55–G66, doi: 10.1190/geo2011-0388.1.